# Excited states built on the $6^-$ isomer in $^{86}_{37}Rb_{49}$

G. Winter, R. Schwengner, J. Reif, and H. Prade
*Institut für Kern- und Hadronenphysik, Forschungszentrum Rossendorf, D-01314 Dresden, Germany*

J. Döring
*Department of Physics, Florida State University, Tallahassee, Florida 32306*

R. Wirowski, N. Nicolay, and P. von Brentano
*Institut für Kernphysik, Universität zu Köln, D-50937 Köln, Germany*

H. Grawe and R. Schubart
*Hahn-Meitner-Institut Berlin, D-14109 Berlin, Germany*
(Received 15 November 1993)

High-spin states of the doubly-odd nucleus $^{86}$Rb containing 37 protons and 49 neutrons have been investigated via the reaction $^{82}$Se($^7$Li, $3n$) using $^7$Li ions with energies between 30 and 35 MeV. The new level scheme is based on prompt $\gamma\gamma$ coincidences, angular distributions and directional correlation orientation ratios of $\gamma$ rays as well as on linear polarizations of some strong $\gamma$ rays and contains levels with excitation energies up to 7.9 MeV and tentative spins up to $16\hbar$. For fifteen of the levels lifetimes in the ps region have been determined by analyzing the Doppler shift of $\gamma$ rays. Several fast $M1$ transitions with $B(M1)\gtrapprox 0.3$ W.u. have been identified. The new high-spin level scheme of $^{86}$Rb is interpreted on the basis of shell-model calculations in the configuration space $1p_{3/2}, 0f_{5/2}, 1p_{1/2}$, and $0g_{9/2}$ for the protons and $1p_{1/2}, 0g_{9/2}$, and $1d_{5/2}$ for the neutrons. The energies of the observed levels with $I > 5$ as well as most of the observed electromagnetic transition probabilities could be well described. The excitation of a $0g_{9/2}$ neutron over the $N$=50 shell gap into the $1d_{5/2}$ orbital is predicted to cause remarkable alterations only for states with $I^\pi \geq 15^+$. Some of the reduced $M1$ transition probabilities calculated within the shell model are found to depend critically on the parametrization used to describe the residual interaction.

PACS number(s): 23.20.−g, 21.60.Cs, 27.50.+e

## I. INTRODUCTION

Yrast states of high spin in doubly-odd Rb nuclei are dominated by the two-particle configurations resulting from the coupling of a $0g_{9/2}$ proton and a $0g_{9/2}$ neutron orbital. For the light isotope $^{80}$Rb a collective band up to spin $15\hbar$ built on this configuration has been found [1] revealing the feature of signature inversion (see, e.g., Ref. [2]) at spin $11\hbar$. This phenomenon is possibly connected with a rearrangement between particle and collective angular momenta. For Rb nuclei with a greater number of neutrons, $^{82,84}$Rb, information on high-spin states is only known up to spin $10\hbar$ [3, 4], and an analysis of the relation between the collective and the particle angular momentum in the high-spin excitations of these nuclei is rather difficult. A level scheme of high-spin states for the even heavier nucleus $^{86}$Rb is up to now not available. This nucleus contains only one proton and one neutron less than the nucleus $^{88}$Sr that is often considered as an inert core in shell-model calculations. Therefore, the properties of high-spin states in $^{86}$Rb formed by the coupling of different particle angular momenta can be analyzed using the shell model. In order to investigate high-spin states in that nucleus an in-beam study of $^{86}$Rb has been initiated. Excited states in $^{86}$Rb have previously been studied in $(n,\gamma)$, in $(p,n)$, and in different particle transfer-reaction experiments (see the recent compilation of Müller and Tepel [5]). Levels decaying to the long-lived $6^-$ isomer at 556.0 keV were unknown except for a $(7)^-$ level at 779.5 keV.

Preliminary results on the level scheme of high-spin states in $^{86}$Rb as found in the present work have been published elsewhere [6].

## II. EXPERIMENTAL PROCEDURES AND RESULTS

Excited states in $^{86}$Rb have been identified using in-beam $\gamma$-ray spectroscopy in connection with the $^{82}$Se($^7$Li,$3n$) reaction at the cyclotron in Rossendorf and the FN Tandem accelerator in Cologne. Angular distributions and linear polarizations of $\gamma$ rays as well as $\gamma\gamma$ coincidences have been measured during the bombardment of $^{82}$Se foils (enriched to 92%, thickness 5 mg cm$^{-2}$) with 35 and 32 MeV $^7$Li ions. In these experiments $\gamma$ rays belonging to the three final nuclei $^{83}$Br, $^{85}$Rb, and $^{86}$Rb are produced with similar intensities. The $\gamma$ rays arising from levels in $^{83}$Br could be identified on the basis of prompt coincidences with $\alpha$ particles emitted during the formation of that nucleus [7]. A clear distinction be-

 

tween $\gamma$ rays belonging to $^{86}$Rb and those of $^{85}$Rb was observed when the bombarding energy was reduced from 35 to 30 MeV. When normalized to the strong 514 keV line of $^{85}$Rb the intensities of the strong lines assigned now to $^{86}$Rb rise by approximately a factor of 3 for the reduced beam energy.

In order to study the angular distributions of the $\gamma$-ray intensities singles $\gamma$-ray spectra have been measured at observation angles of 35°, 90°, 110°, 130°, and 145° with a Ge detector of 10% relative efficiency. This experiment has been carried out at the Rossendorf Cyclotron using a 35 MeV $^{7}$Li beam. The normalization was obtained by assuming an isotropic angular distribution for the isomeric 514 keV $\gamma$ ray in $^{85}$Rb. Unfortunately, several lines assigned to $^{86}$Rb are hidden in complex groups and, therefore, angular distribution coefficients could be derived only for some intense transitions (see Table I). Previously a measurement at the observation angles 37°, 90°, 120°, and 143° was carried out for the study of the Doppler shifts of $\gamma$ rays in $^{85}$Rb [8]. This data set has been analyzed also for angular distributions of $\gamma$ rays in $^{86}$Rb and the results are found to be in fair agreement with the values given in Table I. The $\gamma$-ray intensities have been determined from the isotropic part of the angular distribution, from the singles spectrum measured at 130° or from the intensities in the $\gamma\gamma$ coincidence spectrum gated by the 125.2 keV transition. The results obtained are given in Table I.

The measurement of the linear polarization of $\gamma$ rays carried out in conjunction with our experiments on excited states in $^{85}$Rb [7] has also been analyzed with respect to some strong $\gamma$ rays in $^{86}$Rb. In this experiment an $^{82}$Se powder target of 30 mg cm$^{-2}$ thickness was bombarded with 35 MeV $^{7}$Li ions from the Rossendorf Cyclotron, and the $\gamma$ rays were detected using a plate-shaped Ge(Li) detector of dimensions 27×27×5 mm$^3$. Two singles spectra were measured, one for a parallel and one for a perpendicular orientation of this detector to the reaction plane. The normalization of these measurements was obtained by assuming a vanishing polar-

TABLE I. Energies, intensities, angular distributions, linear polarizations, and DCO ratios for $\gamma$ rays assigned to $^{86}$Rb and energies of the inital states and transition assignments.

| $E_\gamma^a$ (keV) | $I_\gamma^{b,c}$ | $A_2$ | $A_4$ | $P_{expt.}^d$ | $R^e$ | $R^f$ | $E_x$ (keV) | $I_i^\pi$ | $I_f^\pi$ |
|---|---|---|---|---|---|---|---|---|---|
| 125.2 | 62[b] | −0.28(2) | −0.04(3) | −0.35(8) | - | 0.71(3) | 1683.6 | $8^+$ | $7^+$ |
| 129.9 | 34[b] | −0.28(2) | −0.04(4) | −0.36(11) | 1.00(2) | 0.68(2) | 3411.7 | $11^+$ | $10^+$ |
| 144.4 | 2.6[b] | −0.3(2) | - | - | 0.99(6) | - | 3281.8 | $10^+$ | $(9^+)$ |
| 224.3 | 100[b] | −0.41(5) | 0.04(8) | - | 0.99(3) | 0.63(2) | 780.3 | $7^-$ | $6^-$ |
| 263.8 | 4.0[c] | - | - | - | 0.94(6) | 0.58(7) | 5557.2 | $(13^-)$ | $(12^-)$ |
| 287.7 | 1.4[b] | −0.4(1) | - | - | 0.91(8) | - | 3865.9 | $(11^+)$ | $(10^+)$ |
| 331.5 | 28[c] | −0.31(4) | 0.00(5) | −0.40(20) | 0.97(5) | 0.65(3) | 3743.2 | $12^+$ | $11^+$ |
| 447.0 | 1.4[b] | - | - | - | 0.7(2) | 0.4(3) | 7859.9 | (16) | (15) |
| 556.2 | 5.6[c] | - | - | - | 0.95(8) | 0.6(2) | 6113.4 | $(14^-)$ | $(13^-)$ |
| 685.9 | 2.3[c] | - | - | - | - | - | 6799.3 | $(15^-)$ | $(14^-)$ |
| 732.8 | 42[b] | −0.25(7) | - | - | 0.89(7) | - | 2416.4 | $9^+$ | $8^+$ |
| 778.1 | 63[b] | 0.46(11) | 0.3(2) | - | 1.54(5) | 1.2(2) | 1558.4 | $7^+$ | $7^-$ |
| 865.4 | 17[b] | −0.34(5) | - | - | 1.05(6) | - | 3281.8 | $10^+$ | $9^+$ |
| 903.6 | 6.5[b] | −0.2(1) | 0.1(2) | - | - | 0.9(2) | 1683.6 | $8^+$ | $7^-$ |
| 957.3 | 1.5[c] | - | - | - | 1.3(3) | - | 7412.9 | (15) | $(14^+)$ |
| 973.7 | 8.5[c] | - | - | - | 1.0(1) | 0.6(2) | 4716.9 | $13^+$ | $12^+$ |
| 995.4 | 2.5[c] | - | - | - | 1.3(2) | - | 3411.7 | $11^+$ | $9^+$ |
| 1002.4 | 12[b] | −0.17(5) | 0.06(8) | - | 0.99(3) | 0.8(2) | 1558.4 | $7^+$ | $6^-$ |
| 1161.8 | 4.9[b] | - | - | - | 0.9(1) | - | 3578.2 | $(10^+)$ | $9^+$ |
| 1427.5 | 0.5[c] | - | - | - | - | - | 5293.4 | $(12^-)$ | $(11^+)$ |
| 1453.7[g] | 6.5[c] | - | - | - | 0.6(1) | - | 3137.3 | $(9^+)$ | $8^+$ |
| 1598.2 | 19[b] | 0.07(12) | −0.2(2) | - | 1.59(7) | - | 3281.8 | $10^+$ | $8^+$ |
| 1738.7 | 2.8[c] | - | - | - | 1.4(3) | - | 6455.6 | $(14^+)$ | $13^+$ |
| 1814.1 | 3.6[c] | - | - | - | 1.0(2) | - | 5557.2 | $(13^-)$ | $12^+$ |
| 1881.7 | 5.7[c] | - | - | - | 0.8(2) | 0.5(2) | 5293.4 | $(12^-)$ | $11^+$ |
| 1894.7 | 1.2[c] | - | - | - | - | - | 3578.2 | $(10^+)$ | $8^+$ |

[a]Energies of $\gamma$-ray transitions. The errors are between 0.1 and 0.3 keV.

[b]Relative $\gamma$-ray intensities deduced from singles measurements. Errors are between 5 and 10%.

[c]Relative $\gamma$-ray intensities deduced from $\gamma\gamma$ coincidence measurements. Errors are between 10 and 15%.

[d]Experimental values of the linear polarization of $\gamma$ rays.

[e]Ratios of directional correlations of $\gamma$ rays in coincidence with the 125.2 keV $\gamma$ ray.

[f]Ratios of directional correlations of $\gamma$ rays in coincidence with the 1598.2 keV $\gamma$ ray.

[g]This line is part of a doublet with a 1452.7 keV $\gamma$ ray (see text).

ization for the isomeric 514 keV $\gamma$ ray in $^{85}$Rb. Further information on the evaluation of the polarization measurement is given in Ref. [9]. The results obtained are given in Table I.

The measurement of $\gamma\gamma$ coincidences was carried out at the FN Tandem accelerator in Cologne using six Ge detectors in the OSIRIS-CUBE [10] arrangement. A $^{82}$Se foil of 5 mg cm$^{-2}$ thickness (enrichment 92%) was bombarded with 32 MeV $^{7}$Li ions and the $\gamma$ radiation was measured with two Ge detectors at each of the observation angles of 45°, 90°, and 135°. (Details on the placement of the Ge detectors can also be seen in the paper of Schimmer *et al.* [11].) The events have been sorted into a total matrix and, in addition, into different submatrices according to the observation angles. From these submatrices information on the directional correlations of coincident $\gamma$ rays from oriented nuclei has been derived. Furthermore, the Doppler shifts of $\gamma$-ray energies in coincidence spectra derived from submatrices belonging to observation angles of 45° and 135° have been analyzed and lifetimes of excited states have been deduced by the Doppler shift attenuation method. In the total $\gamma\gamma$ coincidence matrix about $3 \times 10^8$ events are collected. Some examples of background-corrected $\gamma\gamma$ coincidence spectra selected from the total matrix are shown in Figs. 1 and 2.

### A. Directional correlations

Directional correlations of coincident $\gamma$ rays from oriented nuclei (DCO ratios) provide information on the multipole orders of the transitions as well as the spins of the levels involved. Since these ratios are derived from $\gamma\gamma$ coincidence spectra the uncertainties arising from overlapping lines should be much smaller than in the conventional angular distribution experiments. DCO ratios have been derived from those submatrices containing only coincidences of a $\gamma$ ray detected at 90° with a $\gamma$ ray detected at 45° or 135°. There are eight such detector combinations in the data set.

For a coincidence pair $\gamma_1 \otimes \gamma_2$ the DCO ratio has been derived from two coincidence intensities $Y$ measured at different observation angles. Directional correlations between the two $\gamma$ rays are reflected in a change of the intensity due to an interchange of the observation angles for $\gamma_1$ and $\gamma_2$. Thus, the DCO ratio reads

$$R(\gamma_1,\gamma_2) = \frac{Y(\gamma_1(\text{detected at } 90°), \gamma_2(\text{detected at } 45° \text{ or } 135°))}{Y(\gamma_1(\text{detected at } 45° \text{ or } 135°), \gamma_2(\text{detected at } 90°))}.$$

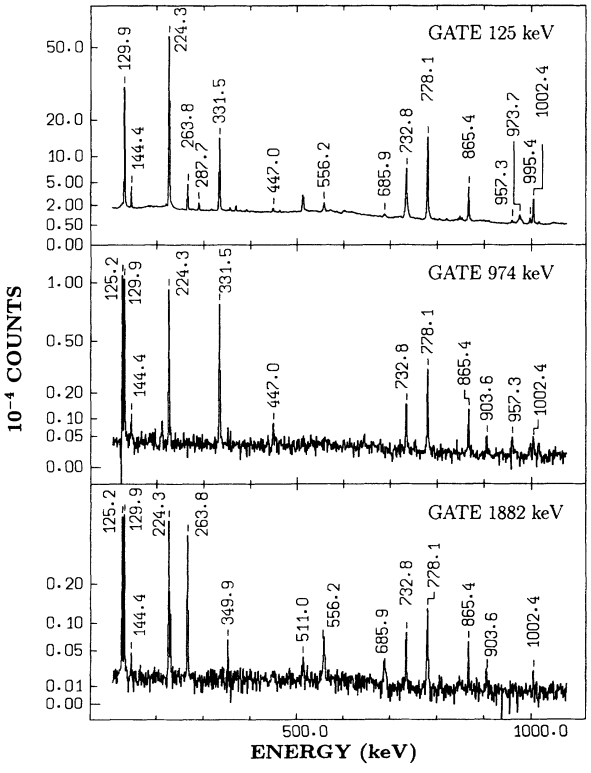


FIG. 1. Examples of $\gamma\gamma$ coincidence spectra derived from the total matrix. Only portions between 100 keV and 1 MeV are shown. For the high-energy portions see Fig. 2. The peaks at 228.1 and 349.9 keV in the lowest spectrum belong to $^{85}$Rb.

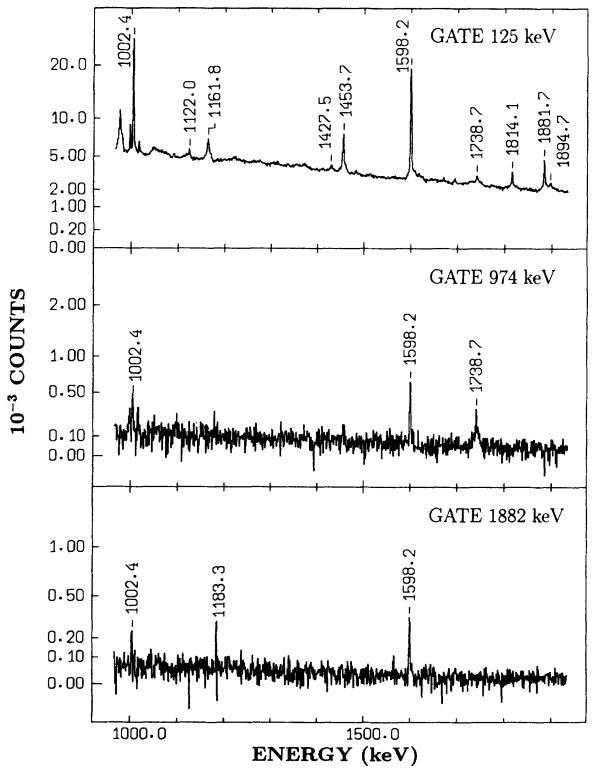


FIG. 2. Examples of $\gamma\gamma$ coincidence spectra derived from the total matrix. Only portions between 1 MeV and 2 MeV are shown. For the low-energy portions see Fig. 1. The peak at 1183.3 keV in the lowest spectrum belongs to $^{85}$Rb.

In order to determine the intensity $Y$ coincidence spectra have been derived for a gate at $E_{\gamma_1}$ from each of the eight submatrices and these spectra have been summed up after subtraction of coincidences arising from the continuum and correction for the individual detector efficiencies. The same procedure has been applied to the transposed submatrices for the determination of $Y$ for interchanged observation angles.

For this geometry, completely aligned nuclei, radiations of pure multipole order $L$, and spin differences $\Delta I$ the following typical values of $R$ are expected [12]:

$$R([L = 1, \Delta I = \pm 1], [L = 1, \Delta I = \pm 1]) = 1 ,$$
$$R([L = 1, \Delta I = \pm 1], [L = 2, \Delta I = \pm 2]) \approx 1.6 ,$$
$$R([L = 2, \Delta I = \pm 2], [L = 1, \Delta I = \pm 1]) \approx 0.6 ,$$
$$R([L = 2, \Delta I = \pm 2], [L = 2, \Delta I = \pm 2]) = 1 .$$

If the multipole order and the spin of the initial and the final states for the gate transition $\gamma_1$ are known, experimental values of this intensity ratio $R$ allow us to assign values of $L$ and/or $\Delta I$ for the second transition in the cacscade.

Reliable experimental values have, however, only been obtained for the gate transitions 125.2, 129.9, 331.5, and 1598.2 keV since these $\gamma$ rays are rather well separated from other peaks and do not show a strong Doppler shift. The results obtained for the gates at 125.2 keV and 1598.2 keV are given in Table I. The data obtained are consistent with the spin assignments.

### B. Doppler shift attenuation analysis

In order to analyze Doppler shifts of $\gamma$ rays in $^{86}$Rb coincidence spectra derived from the corresponding submatrices have been summed up for each of the observation angles 45° and 135° separately. Gates have been set on the strong transitions at 125.2, 129.9, and 331.5 keV. Lifetimes of excited states have been derived by comparing the observed line shapes with calculated line shapes based on a Monte Carlo calculation of the velocity distribution of the emitting nuclei. In this calculation reactions in different depths of the target, the kinematics of an evaporation reaction as well as the slowing down and deflection of the recoiling nuclei are taken into account. For the slowing-down process Lindhard's cross sections [13] have been used with correction factors $f_e$=0.9 and $f_n$=0.7 for the electronic and nuclear stopping powers, respectively. The same description of the calculated lineshapes has already been used to analyze the Doppler shift of $\gamma$ rays in $^{85}$Rb [8].

In order to estimate the side-feeding time for the population of states at high excitation energy it is assumed that the side-feeding time vanishes for states which might be directly populated in the reaction (entry states). The excitation energy of those states can be estimated from the kinematics of the reaction under the assumption of an average kinetic energy of 2.5 MeV for each evaporated neutron. Levels below that energy are populated via more and more intermediate nuclear states, and an increase of the side-feeding time with decreasing excitation energy by 0.03 ps MeV$^{-1}$ was assumed. On the basis of these assumptions we estimated earlier the side-feeding time for levels in $^{85}$Rb [8] which are populated after the evaporation of four neutrons from the compound system $^{89}$Rb while the population of states in $^{86}$Rb is accompanied by the evaporation of only three neutrons from the same compound system. In $^{85}$Rb a vanishing side-feeding time was estimated for the highest observed state at 7.1 MeV and was also supported in the analysis of the experimental data [8].

According to these assumptions the side-feeding time in $^{86}$Rb should vanish for states with excitation energies higher than ≈18 MeV, and for the highest observed state at 7.8 MeV a side-feeding time of ≈0.3 ps is expected. However, the analysis of the line shape of the 1738.7 keV peak under the assumption of vanishing side-feeding times for the levels at 7859.9, 7412.9, and 6455.6

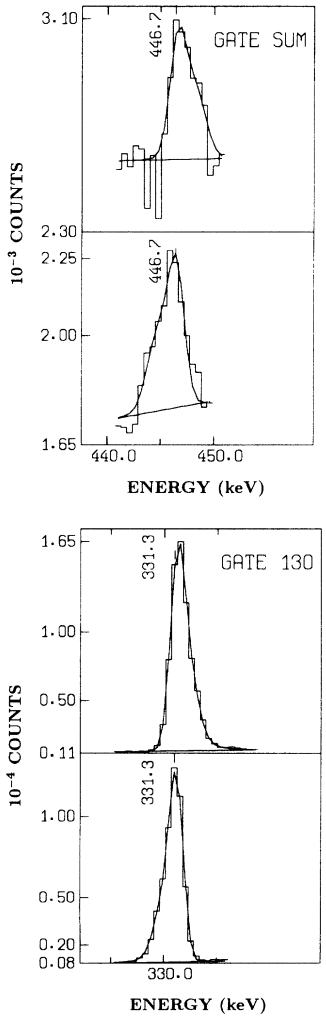


FIG. 3. Illustrations for the line shape analysis for the $\gamma$ rays at 447.0 and 331.5 keV. The line shapes for the two observation angles of 45° and 135° are described in a joint fit. The energy of the transition given in the figure has been found in that analysis. The experimental line shape of the 447.0 keV peak has been taken from a sum of the coincidence spectra gated by the 125 and 331 keV $\gamma$ rays.

keV results in an apparent lifetime of 0.2 ps for the 6455.6 keV level. Therefore, it is reasonable to assume that the side-feeding time for this level is not longer than 0.2 ps. Furthermore, it is rather unlikely that the side-feeding time for the level at 6799.3 keV is longer than 0.4 ps since the analysis of the line shape of the 685.9 keV $\gamma$ ray without feeding correction results in an apparent lifetime of only 0.5 ps. Based on these arguments we applied a side-feeding time of 0.15 ps for the level at 7.8 MeV. For states at lower excitation energies $E_x$ the side-feeding time was increased by $0.03[7.8 - E_x(\mathrm{MeV})]$ ps.

It should be mentioned that an increase of the side-feeding time with decreasing excitation energy by approximately 0.05 ps $\mathrm{MeV}^{-1}$ has been derived [14] in a detailed study of experimental line shapes of $\gamma$ rays in $^{75}$Br. In that analysis the side-feeding time vanishes for excitation energies higher than 5 MeV while levels are identified up to 7 MeV and the energy of the entry states is even higher than 10 MeV.

Experimental and calculated line shapes are compared for the observation angles 45° and 135° in a joint fit. Typical examples of such analyses are shown in Figs. 3, 4, and 5. Including two line shapes in a joint fit requires one additional normalization parameter to describe the ratio between the efficiencies of the detectors positioned at the two observation angles. Due to the symmetry of these angles with respect to 90° the two line shapes are symmetric with respect to a reflection at the energy of the transition. In this way, the influence of interfering peaks or of other distortions in the experimental spectra is remarkably reduced.

The lifetime of the 3411.7 keV level could not be determined directly due to the rather small energy shift expected for the 129.9 keV $\gamma$ ray. Therefore, the evaluation of lifetimes for the lower-lying levels at 3281.8 and 2416.4 keV is hindered. As we know from the polarization measurement that the 129.9 keV transition is of multipolarity $M1$ a lower limit for the lifetime of the 3411.7 keV

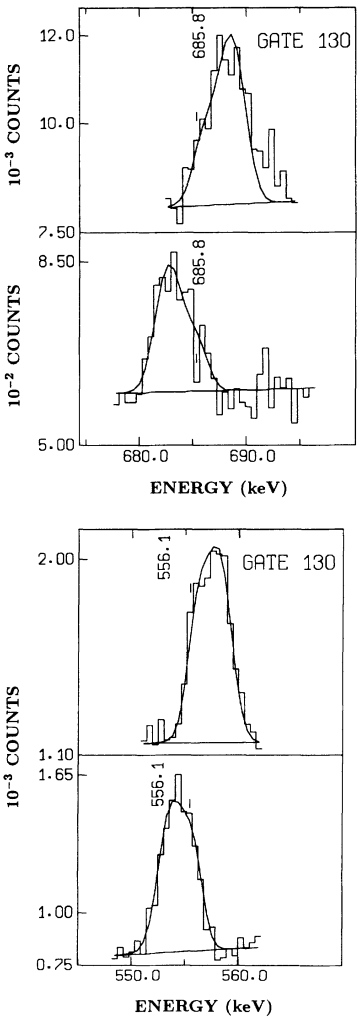


FIG. 4. Illustrations for the line shape analysis for the $\gamma$ rays at 685.9 and 556.2 keV. The line shapes for the two observation angles of 45° and 135° are described in a joint fit. The energy of the transition given in the figure has been found in that analysis.

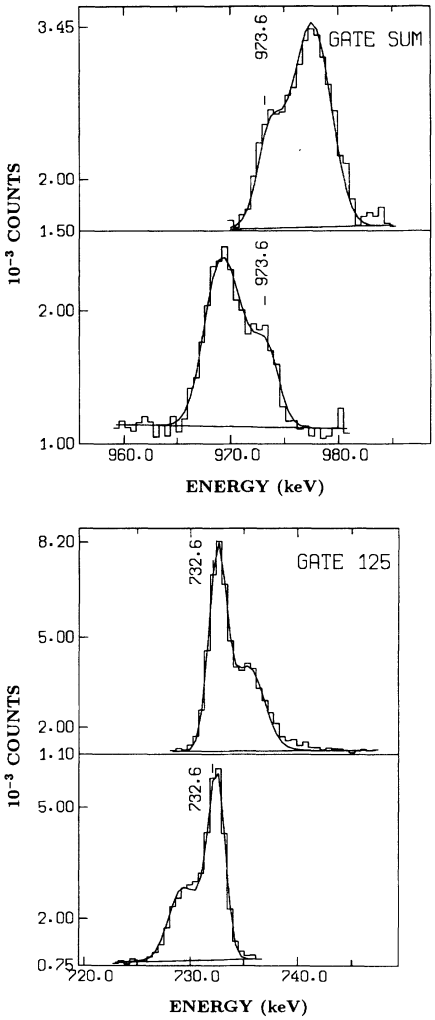


FIG. 5. Illustrations for the line shape analysis for the $\gamma$ rays at 973.7 and 732.8 keV. The line shapes for the two observation angles of 45° and 135° are described in a joint fit. The energy of the transition given in the figure has been found in that analysis.

level ($\tau \geq 7$ ps) can be estimated by assuming an upper limit of $B(M1) \leq 2$ Weisskopf units (W.u.) for that transition. The specific value of a lifetime in the region of 7 ps for a feeding level has only little influence on the analysis of the Doppler shift for the $\gamma$ rays emitted from lower-lying levels because the recoiling nuclei are already stopped after some picoseconds. Based on the assumption of 7 ps for the lifetime of the 3411.7 keV level we derived a lifetime of less than 1 ps for the level at 3281.8 keV from the line shapes of the 865.4 and 1598.2 keV $\gamma$ rays in the coincidence spectrum gated by the 125.2 keV $\gamma$ ray. Considering, however, the line shapes of the two transitions deexciting the 3281.8 keV level in the coincidence spectrum gated by the 129.9 keV transition we observe the implications of the long lifetime of the 3411.7 keV level since we know that the lifetime of the 3281.8 keV level itself is much smaller and other populations of the 3281.8 keV level are excluded. In this way we determined values of $\tau$ =10(1) ps and $\tau$ =7(1) ps for the lifetime of the 3411.7 keV level from the line shapes of the 865.4 keV and 1598.2 keV $\gamma$ rays, respectively, and an average lifetime of $\tau_{av}$=8(2) ps is adopted. The experimental lifetimes for levels in $^{86}$Rb are given in Table II.

## III. THE LEVEL SCHEME

The information derived from the present experiments is summarized in the level scheme for $^{86}$Rb shown in Fig. 6. Based on the results of prompt $\gamma\gamma$ coincidences a new cascade of eleven $\gamma$ rays is established (see Figs. 1 and 2). This cascade is assigned to populate the long-lived $6^-$ isomer in $^{86}$Rb as derived from both the relative excitation function and the nonobservation of these lines in particle-$\gamma$ coincidence experiments [7]. Spin and parity assignments given in Fig. 6 are deduced from the results of the angular distribution, directional correlation, and polarization measurements for $\gamma$ rays (see Table I).

From previous work (see the compilation [5]) the assignments of spin and parity $6^-$ and $(7)^-$ to the isomeric level at 556.0 keV and to a level at 779.5 keV, respectively, were known. A level at 779.5 keV was observed in

TABLE II. Lifetimes in $^{86}$Rb.

| $E_{level}$ (keV) | $E_\gamma$ (keV) | $B$[a] % | $\tau$[b] (ps) Gate 125 keV | $\tau$[b] (ps) Gate 130 keV | $\tau$[b] (ps) Gate sum[c] | Lifetime[b] (ps) Adopted[d] |
|---|---|---|---|---|---|---|
| 7859.9 | 447.0 | 100 | - | - | 1.0(1) | 1.0(2/3) |
| 7412.9 | 957.3 | 100 | - | - | 0.6(1) | 0.6(1/2) |
| 6799.3 | 685.9 | 100 | 0.29(3) | 0.25(3) | - | 0.3(1/2) |
| 6455.6 | 1738.7 | 100 | 0.05(4) | 0.05(3) | 0.02(3/2) | 0.05(6/4) |
| 6113.4 | 556.2 | 100 | 0.36(2) | 0.31(2) | - | 0.4(1/2) |
| 5557.2 | 263.8 | 53(5) | 1.3(1) | 1.2(1) | - | 1.1(2/3) |
| - | 1814.1 | 47(5) | - | - | 0.8(1) | - |
| 5293.4 | 1881.7 | 92(9) | 0.35(5) | 0.44(6) | - | 0.5(1/2) |
| 4716.9 | 973.7 | 100 | 0.12(1) | 0.11(1) | 0.12(1) | 0.12(5/7) |
| 3865.9 | 287.7 | 100 | 1.8(5) | - | - | 1.8(5) |
| 3743.2 | 331.5 | 100 | 1.8(1) | 1.9(1) | - | 1.9(2) |
| 3578.2 | 1161.8 | 80(6) | 0.32(3) | - | - | 0.4(1/2) |
| - | 1894.7 | 20(5) | 0.33(4) | - | - | - |
| 3411.7 | 129.9 | 93(2) | - | 8(2)[e] | - | 8(2)[e] |
| - | 995.4 | 7(2) | - | - | - | - |
| 3281.8 | 865.4 | 44(5) | 1.2(2) | - | - | 1.0(2) |
| - | 1598.2 | 49(5) | 0.8(1) | - | - | - |
| - | 144.4 | 7(2) | - | - | - | - |
| 3137.3 | 1453.7[f] | 100 | 0.8(1) | - | - | 0.8(2) |
| 2416.4 | 732.8 | 100 | 0.35(1) | - | - | 0.4(1) |

[a]Branching ratio of the $\gamma$ rays deexciting the level at the energy given in the first column.
[b]Lifetimes obtained in this analysis. The errors are given in parentheses in units of the last decimal. When asymmetric the notation is (upper/lower) uncertainty. Only statistical errors are given. The lifetimes depend on the assumptions on the side-feeding time (see text).
[c]Coincidence spectrum obtained by adding the spectra belonging to the gates at 125, 130, and 331 keV.
[d]Errors are given in parentheses in units of the last decimal. When asymmetric the notation is (upper/lower) uncertainty. The errors of the adopted values include uncertainties of 10% for the stopping power and $\pm$0.1 ps for the side-feeding time.
[e]This lifetime has been determined from the line shapes of the 865.4 and 1598.2 keV $\gamma$ rays in the coincidence spectrum gated by the 129.9 keV $\gamma$ ray (see text).
[f]This line is part of a doublet with a 1452.7 keV $\gamma$ ray (see text).

different particle-transfer reactions but a $\gamma$ ray with energy 223.9(10) keV connecting these two states was only observed in a $(n,\gamma)$ study. In the present work a strong 224.3 keV transition was found as the most intense $\gamma$ ray in the new cascade and placed directly onto the isomer. The experimental value of the angular distribution coefficient $A_2$ of this $\gamma$ ray points to a $\Delta I = 1$ dipole transition with a small admixture of quadrupole radiation. Since for that low-energy transition an $E2$ admixture is more likely than an $M2$ admixture we assign $I^\pi = 7^-$ to that level. This assignment is supported by a strong $L = 4$ population of that state in the $(d,p)$ reaction on the $\frac{5}{2}^-$ ground state of $^{85}$Rb [5]. According to the $\gamma$-ray energy determined in this work for the 224.3 keV transition the level energy reads now 780.3 keV.

The positive $A_2$ value of the 778.1 keV $\gamma$ ray is interpreted as arising from an $L=1$ transition between states of the same spin. This assignment is also supported by the observation of a negative $A_2$ value for the 1002.4 keV crossover transition to the isomeric $6^-$ state. The results of both the angular distribution and the linear polarization measurements reveal the multipolarity $M1$ for the 125.2 keV transition connecting levels differing in spin by $1\hbar$. Therefore, the two states at 1558.4 and 1683.6 keV belong to the same parity. We assign positive parity to these two states since in that case the nonobservation of a transition from the upper level ($8^+$ level) to the $6^-$ isomer might be related to the $M2$ multipolarity. Positive parity is also assigned to the levels at 2416.4, 3137.3, 3281.8, 3411.7, 3743.2, and 4716.9 keV. Among the transitions connecting these states the multipolarity $M1$ is deduced for the 129.9 and 331.5 keV $\gamma$ rays from the results of the linear-polarization measurement. In addition, the assignment of the multipolarity $M1$ to the transitions at 129.9, 144.4, 331.5, 732.8, and 973.7 keV is strongly suggested from the reduced electromagnetic transition probabilities since the assumption of $E1$ transitions would lead to $B(E1)$ values greater than $10^{-3}$ W.u. which is the greatest $B(E1)$ value observed in this mass region (see, e.g., the compilation [15]). The DCO ratio derived for the 1598.2 keV crossover transition points to a stretched quadrupole transition while for the other strong transitions in this level sequence stretched dipole transitions are indicated.

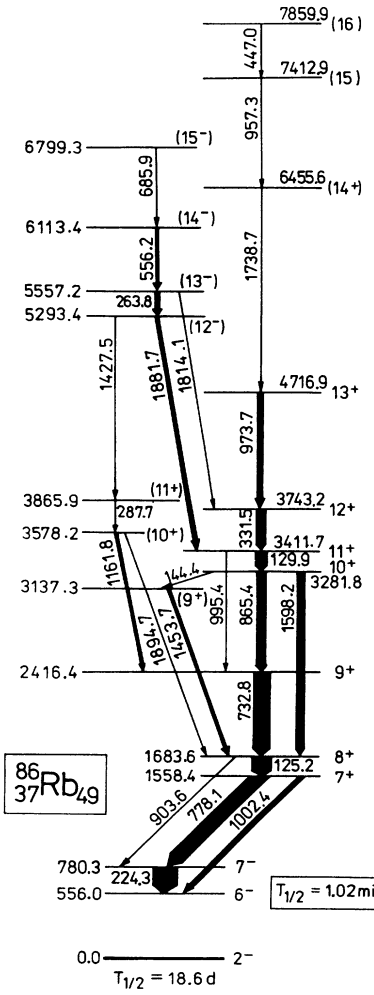


FIG. 6. Level scheme of $^{86}$Rb deduced in the present in-beam study. Levels built on the ground state (see the compilation in Ref. [5]) are omitted.

While the assignment of the same parity to all states of this sequence is well established from the analysis of our data the preference of positive parity is mainly derived from systematics. If all these states would belong to negative parity the absence of all low-lying high-spin states of positive parity in this study cannot be explained. The strong Doppler shift of the weak 1738.7 keV transition hinders us to derive precise DCO information. The lifetime of the 6455.6 keV level could only be determined with large uncertainty. Nevertheless, the reduced electromagnetic transition probability derived for the 1738.7 keV transition favors an $M1$ assignment for this transition. The assumption of the multipolarity $E1$ would again lead to a $B(E1)$ value greater than $10^{-3}$ W.u. Thus, the spin and parity assignments for the upper levels in this level sequence is less accurate.

The population intensities of the levels at 6799.3 and 6113.4 keV indicate that these levels might be yrast states. The reduced transition probabilities determined for the 685.9, 556.2, and 263.8 keV $\gamma$-ray transitions strongly suggest $M1$ multipolarity for these three transitions because the assumption of the multipolarity $E1$ would imply that their $B(E1)$ values should exceed the greatest $B(E1)$ value observed in this mass region (see, e.g., the compilation [15]).

The main intensity depopulating these levels flows via the 1881.7 keV $\gamma$ ray to the $11^+$ level at 3411.7 keV. Unfortunately, a decision between the multipole types $M1$ and $E1$ for this transition cannot be derived from our data. Based on the DCO ratios of the 263.8 and 556.2 keV $\gamma$ rays determined from the coincidence intensities with the 129.9 keV $\gamma$ ray we propose the spins (14), (13), and (12) for the levels at 6113.4, 5557.2, and 5293.4 keV, respectively. In addition, spin (15) is proposed for the level at 6799.3 keV due to the multipolarity $M1$ suggested for the 685.9 keV $\gamma$ ray from the lifetime measurements. From a comparison with predictions of shell-model calculations (see Sec. IV) an assignment of negative parity to this group of states is very likely. This

assignment implies the multipolarity $E1$ for the transitions at 1814.1 and 1881.7 keV. From the experimental lifetimes of the levels at 5557.2 and 5293.4 keV (see Table II) values of $B(E1)= 3.6\times10^{-5}$ W.u. and $1.5\times10^{-4}$ W.u., respectively, have been derived for these transitions.

In addition, the level at 5293.4 keV decays via a cascade of transitions at 287.7 and 1427.5 keV to a $(10^+)$ level at 3578.2 keV that is well established due to the transitions of 1161.8 and 1894.7 keV to the $9^+$ and $8^+$ levels, respectively. Spin and parity $(11^+)$ are tentatively assigned to the level at 3865.9 keV on the basis of the angular distribution measurement as well as the reduced transition probability of the 287.7 keV transition.

The peak at 1453 keV is identified as a doublet formed from the two close-lying lines at 1452.7 and 1453.7 keV that have been observed in the coincidence spectra gated by the 732 keV and 125 keV transitions, respectively. The coincidence spectrum gated by the doublet at 1453 keV indicates that only 25% of the intensity of the doublet belongs to the 1452.7 keV component which obviously feeds to the $9^+$ level. Since other information on the placement of this component has not been obtained, it is not included in the level scheme. The intensity relation between the two components has been used in the analysis of the Doppler shift of the 1453.7 keV $\gamma$ ray in the coincidence spectrum gated by the 125 keV transition. The assignment of $(9^+)$ to the level at 3137.3 keV is based on both the decay to the $8^+$ level and the large $B(M1)$ value for the 144.4 keV transition populating this level from the $10^+$ level.

## IV. SHELL-MODEL CALCULATIONS

The nucleus $^{86}$Rb is formed from 37 protons and 49 neutrons. In the spherical shell model, both these numbers of particles fill almost all levels up to a marked energy gap between successive levels. This situation makes numerical calculations within the shell model easier since only some orbitals below that gap are usually considered as active orbitals. In the following we shall compare our experimental data on high-spin states in $^{86}$Rb with predictions of the shell model. For the calculations the code RITSSCHIL [16] has been employed.

### A. Residual interactions

The model space has been generated out of the active orbitals $0f_{5/2}, 1p_{3/2}, 1p_{1/2}$, and $0g_{9/2}$ for the protons $(\pi)$ and the $1p_{1/2}, 0g_{9/2}$, and $1d_{5/2}$ orbitals for the neutrons $(\nu)$ relative to a hypothetic $^{66}$Ni core.

Since an empirical Hamiltonian for this configuration space is so far not available, it was necessary to combine different empirical Hamiltonians with results obtained from schematic nuclear interactions. (For details see the paper by Winter *et al.* [17] on shell-model calculations in $^{85,86}$Kr.) The effective interaction in the proton shells has been taken from the paper by Ji and Wildenthal [18]. In that work the residual interaction and the single-particle energies of the proton orbitals are found in a least-squares fit to 170 experimental energy levels in $N$=50 nuclei with mass numbers between 82 and 96. For the proton-neutron interaction connecting the $\pi(1p_{1/2}, 0g_{9/2})$ and the $\nu(1p_{1/2}, 0g_{9/2})$ orbitals the data given by Gross and Frenkel [19] have been used who derived the effective nuclear interaction in the $(1p_{1/2}, 0g_{9/2})$ space by an iterative fit to 95 experimentally known energies of states in $N$=48, 49, and 50 nuclei. The matrix elements of the neutron-neutron interaction for the $1p_{1/2}, 0g_{9/2}$ orbitals have been assumed to be equal to the $T$=1 component of the $\pi\nu$ interaction given by Gross and Frenkel [19]. For the $(\pi 0f_{5/2}, \nu 0g_{9/2})$ residual interaction the matrix elements proposed by Li *et al.* [20] have been applied. The diagonal matrix elements for the $\nu(0g_{9/2}, 1d_{5/2})$ multishell have been taken from the work of Li and Daehnick [21]. They determined the residual interaction by the particle-hole transformation of experimental energies of the multiplet $\nu(0g_{9/2}, 1d_{5/2})$ in $^{88}$Sr. Following Muto *et al.* [22] we calculated the remaining matrix elements involving the $\nu 1d_{5/2}$ orbital with the surface delta interaction (see, e.g., Glaudemans *et al.* [23]). The values of the strength parameters are, in MeV, $A_{T=1} = 0.251$ and $A_{T=0} = 0.318$ [22].

The single-particle energies relative to the $^{66}$Ni core have been derived from the single-particle energies of the proton orbitals given by Ji and Wildenthal [18] with respect to the $^{78}$Ni core, from the neutron single-hole energies of the $1p_{1/2}, 0g_{9/2}$ orbitals [19], and the neutron single-particle energy of the $1d_{5/2}$ shell [22] relative to the $^{88}$Sr core. The transformation of these single-particle energies with respect to the $^{66}$Ni core has been performed [24] on the basis of the effective residual interactions given before. The obtained values are, in MeV, $\epsilon^{\pi}_{f_{5/2}}=-9.106$, $\epsilon^{\pi}_{p_{3/2}}=-9.033$, $\epsilon^{\pi}_{p_{1/2}}=-4.715$, $\epsilon^{\pi}_{g_{9/2}}=-0.346$, $\epsilon^{\nu}_{p_{1/2}}=-7.834$, $\epsilon^{\nu}_{g_{9/2}}=-6.749$, $\epsilon^{\nu}_{d_{5/2}}=-4.144$.

These single-particle energies and the corresponding values for the strengths of the residual interactions (in the following this parameter set is called PARSET-A) have been used to calculate level energies as well as $M1$ and $E2$ transition probabilities.

For comparison, additional calculations have been carried out using a new parametrization of the considered effective nuclear interaction [25] (later on called PARSET-B). This model space is generated out of the $0g_{9/2}, 1p_{1/2}, 1p_{3/2}$, and $0f_{5/2}$ proton and neutron hole-orbitals with respect to the doubly closed $^{100}_{50}$Sn core, and the Kuo-Brown method [26] was applied to calculate the $T$=1 and $T$=0 components of the effective two-body interaction while the one-hole energies have been determined by a least-squares fit to experimental energies.

### B. Configuration space

Due to the large number of active orbitals a truncation of the model space was necessary to make the calculation feasible. In a first step the neutron configurations have been restricted to the $0g_{9/2}$ orbital and the $1p_{1/2}$ and $1d_{5/2}$ orbitals have been neglected. Considering the proton orbitals only it is sufficient to allow at most three protons to occupy the $0g_{9/2}$ shell [18] while the occupation

of the other proton orbitals is not limited. The coupling of a one-neutron hole excitation in the $0g_{9/2}$ shell to this proton space yields a model space (configuration space I) which has dimensions of up to 7900. The addition of excitations in the $\nu 1p_{1/2}$ orbital to this space results in energy shifts of less than 15 keV for the yrast levels of negative parity with $I \leq 16$ and for yrast as well as yrare levels of positive parity with $7 \leq I \leq 16$. Therefore, the one-hole configuration $\nu(1p_{1/2})^1$ has been neglected in further calculations.

Since we are considering levels with energies up to 7.8 MeV and spins up to $16\hbar$, the inclusion of the $1d_{5/2}$ neutron shell might be of importance. The coupling of the proton configuration $(0f_{5/2}1p_{3/2})^8(0g_{9/2})^1$ to a single neutron hole in the $0g_{9/2}$ shell results in a maximum spin value of $15\hbar$. Positive-parity states with higher spin values can be generated either by lifting three protons to the $0g_{9/2}$ shell or by including the seniority-three neutron excitation $(0g^8_{9/2}1d^1_{5/2})$.

Our results of shell-model calculations for $^{86}$Kr reveal that the breakup of a $0g_{9/2}$ neutron pair and the excitation of one of these neutrons to the $1d_{5/2}$ shell needs approximately 5 MeV. Such neutron excitations carry angular momenta of up to $7\hbar$ and are found to be important for describing high-spin states with spin $\geq 7\hbar$ in $^{86}$Kr [17].

In $^{86}$Rb a maximum increase of the angular momentum by $6\hbar$ might result from lifting the unpaired $0g_{9/2}$ neutron to the $1d_{5/2}$ orbital and breaking additionally a $0g_{9/2}$ neutron pair. In order to include such three-neutron excitations as well as proton excitations with three protons in the $0g_{9/2}$ orbital in the calculations for $^{86}$Rb a severe reduction of the physical configuration space is necessary to handle the matrices on the computer.

For a schematic calculation taking into account the extended neutron space we consider states of positive parity with $I \geq 7$ only. From the nine active protons either six or eight are allowed to occupy orbitals of the negative-parity subshell $(0f_{5/2}, 1p_{3/2}, 1p_{1/2})$ and, correspondingly, three or one proton may occupy the $0g_{9/2}$ orbital. At least four of the protons in the negative-parity subshell are restricted to the $0f_{5/2}$ orbital and at least two protons are assumed to remain in the $1p_{3/2}$ orbital.

Furthermore, the neutron configuration space built up from excitations in the $0g_{9/2}$ and $1d_{5/2}$ orbitals has been truncated by taking into account only those configurations in which the neutrons moving in the $0g_{9/2}$ orbital are coupled to a total angular momentum of at least $\frac{9}{2}\hbar$. In this way neutron configurations of the type $(0g_{9/2})^9_{9/2}(1d_{5/2})^0$ and $(0g_{9/2})^8_{6,8}(1d_{5/2})^1_{5/2}$ are kept while the configurations $(0g_{9/2})^8_{0,2,4}(1d_{5/2})^1_{5/2}$ are omitted. With these restrictions of the proton and neutron configuration spaces a model space with dimensions of less than 12 500 was obtained (configuration space II) for describing high-spin states of positive parity in $^{86}$Rb. A coupling of the neglected three-neutron configurations to the $0g_{9/2}$ proton orbital would lead to positive-parity states with angular momenta up to $11\hbar$. Since the excitation energy of the $11^+$ yrast state is only 3.4 MeV, it is very unlikely that the shell-model description of that state is considerably affected by the neglection of configurations containing both the $1d_{5/2}$ neutron orbital and a broken $0g_{9/2}$ neutron pair.

## V. RESULTS AND DISCUSSION

### A. Results obtained in configuration space I

A comparison of experimentally observed levels with predictions of the shell-model calculations using the parametrization PARSET-A is shown in Fig. 7. In this configuration space excitations of the $\nu 1d_{5/2}$ orbital have been neglected. In agreement with the experimental result the ground state is predicted as the $2^-$ level which is characterized by the coupling of one neutron hole in the $0g_{9/2}$ orbital to the $\pi(0f^5_{5/2}, 1p^4_{3/2})$ configuration. The same structure is prevailed in the wave function of the lowest $7^-$ level whereas the lowest $6^-$ state is predominantly formed by coupling one hole in the $\nu 0g_{9/2}$ orbital to the $\pi(0f^6_{5/2}, 1p^3_{3/2})$ configuration.

The excitation energies of the experimentally known yrast states with $7^+ \leq I^\pi \leq 13^+$ are well reproduced in the calculations. The structure of the wave function of these levels are determined by the residual interaction between the proton and neutron $0g_{9/2}$ orbitals and the

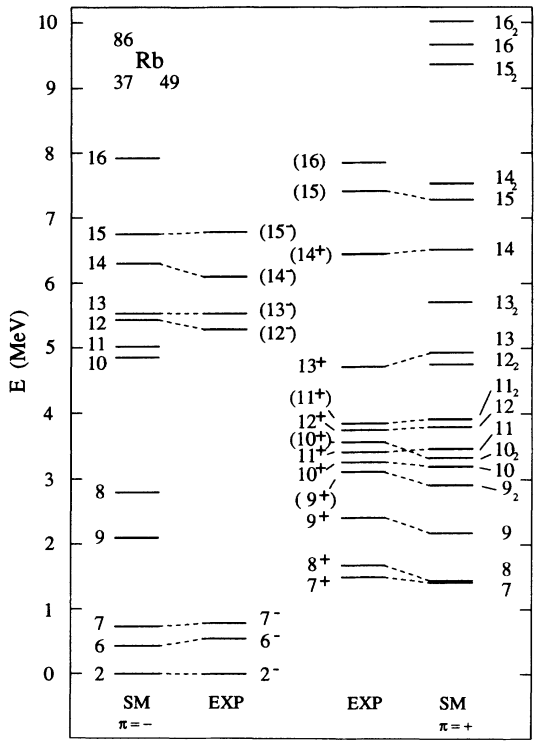


FIG. 7. Comparison of experimental and calculated level energies of $^{86}$Rb using shell-model parameters PARSET-A and configuration space I (see text). From the calculated levels only the ground state, the yrast states with $I^\pi \geq 6^-$ or $I^\pi \geq 7^+$, and the second-lowest states with $I^\pi \geq 9^+$ are shown. Based on the calculated energies only a weak population of the states with $I^\pi = 8^-$ and $9^-$ is expected, and experimental information on these states has not been obtained.

coupling of the $(\pi 0g^1_{9/2}, \nu 0g^9_{9/2})$ configuration to the remaining eight protons occupying the negative-parity orbitals. The $7^+$, $8^+$, and $9^+$ as well as the $10^+$, $11^+$, $12^+$, and $13^+$ yrast states result mainly from the coupling of the $(\pi 0g^1_{9/2}, \nu 0g^9_{9/2})$ configuration to the proton cluster $(0f_{5/2}, 1p_{3/2})^8_J$ where the angular momentum $J$ takes the values $0\hbar$ and $4\hbar$, respectively.

Positive-parity states with higher spin values can be formed by breaking an additional proton pair in the $\pi(0f_{5/2}, 1p_{3/2}, 1p_{1/2})$ subshell and generating the $\pi(0f_{5/2}, 1p_{3/2}, 1p_{1/2})^8_{J=6^+}$ configuration. The coupling of this cluster to the $(\pi 0g^1_{9/2}, \nu 0g^9_{9/2})$ structure results in states with a maximal spin value of $15\hbar$. The excitation of one proton to the $\pi 1p_{1/2}$ orbital explains the rather large energy separation between the $13^+$ and $14^+$ yrast states which is well reproduced in the calculations. In order to form excitations with spins higher than $15\hbar$ in this configuration space a proton pair must be lifted to the $0g_{9/2}$ orbital. Accordingly, the calculations predict a rather large energy separation between the $15^+$ and $16^+$ yrast levels which is not supported by our experimental findings. A description of these high-spin states within an extended neutron configuration space is presented in the next subsection.

The levels observed at 3137.3, 3578.2, and 3865.9 keV correspond very likely to the second-lowest $9^+$, $10^+$, and $11^+$ shell-model states.

The properties of the levels with tentative spins of (12), (13), (14), and (15) observed at 5293.4, 5557.2, 6113.4, and 6799.3 keV, respectively, are found to be in good agreement with the shell-model prediction for yrast states of negative parity (see Fig. 7 and Table III). The description of both, the small level separations and the rather large $B(M1)$ values for the $\Delta I = 1$ transitions between these states point to an assignment of negative parity to these states whereas the second-lowest states of positive parity with the same spin values cannot explain the properties observed for this group of levels.

In order to illustrate the shell-model predictions based on the other set of parameters for the residual interaction [25] we show the level energies calculated with PARSET-B together with the experimental energies in Fig. 8. Again, the predictions for the yrast states of positive parity are in satisfactory agreement with the experiment but the separation between the $7^+$ level and the

TABLE III. Comparison of experimental and calculated transition probabilities in $^{86}$Rb.

| $E_i^{a}$ (keV) | $I_i^\pi \to I_f^\pi$ [b] | $B(\sigma\lambda)^{c}_{expt}$ | $I_i^\pi \to I_f^\pi$ [d] | $B(\sigma\lambda)^{e,f}_{calc}$ | $B(\sigma\lambda)^{g,f}_{calc}$ | $B(\sigma\lambda)^{h,f}_{calc}$ |
|---|---|---|---|---|---|---|
| 7859.9 | $(16) \to (15)$ | 0.4(2/1) | $16^+_1 \to 15^+_1$ | $1.1\times10^{-5}$ | 0.001 | 0.56 |
| 7412.9 | $(15) \to (14^+)$ | 0.06(3/1) | $15^+_1 \to 14^+_1$ | 0.95 | 0.035 | 0.05 |
| 6799.3 | $(15^-) \to (14^-)$ | 0.3(6/1) | $15^-_1 \to 14^-_1$ | 0.54 | 1.70 | - |
| 6455.6 | $(14^+) \to 13^+$ | 0.12(50/1) | $14^+_1 \to 13^+_1$ | 0.001 | 0.006 | 0.10 |
| 6113.4 | $(14^-) \to (13^-)$ | 0.5(5/1) | $14^-_1 \to 13^-_1$ | 0.45 | 2.06 | - |
| 5557.2 | $(13^-) \to (12^-)$ | 0.8(3/1) | $13^-_1 \to 12^-_1$ | 0.53 | 2.49 | - |
| 4716.9 | $13^+ \to 12^+$ | 0.3(4/1) | $13^+_1 \to 12^+_1$ | 0.54 | 0.48 | 0.50 |
| 3865.9 | $(11^+) \to (10^+)$ | 0.7(3/2) | $11^+_2 \to 10^+_2$ | 0.004 | 0.72 | 0.07 |
| 3743.2 | $12^+ \to 11^+$ | 0.46(5/4) | $12^+_1 \to 11^+_1$ | 0.72 | 0.86 | 0.97 |
| 3578.2 | $(10^+) \to 9^+$ | 0.04(4/1) | $10^+_2 \to 9^+_1$ | 0.03 | 0.31 | 0.16 |
| 3578.2 | $(10^+) \to 8^+$ | 0.7(8/2)[i] | $10^+_2 \to 8^+_1$ | 1.50 | 3.56 | 0.51 |
| 3411.7 | $11^+ \to 10^+$ | 1.7(6/4) | $11^+_1 \to 10^+_1$ | 0.71 | 1.17 | 1.37 |
| 3411.7 | $11^+ \to 9^+$ | 0.3(2/1)[i] | $11^+_1 \to 9^+_1$ | 0.01 | 0.42 | 0.02 |
| 3281.8 | $10^+ \to 9^+$ | 0.022(6/4) | $10^+_1 \to 9^+_1$ | 0.43 | 0.05 | 0.62 |
| 3281.8 | $10^+ \to 8^+$ | 1.7(5/3)[i] | $10^+_1 \to 8^+_1$ | 0.02 | 0.84 | 0.04 |
| 3281.8 | $10^+ \to (9^+)$ | 0.7(2/1) | $10^+_1 \to 9^+_2$ | 0.15 | 1.28 | 0.22 |
| 3137.3 | $(9^+) \to 8^+$ | 0.013(5/2) | $9^+_2 \to 8^+_1$ | 0.05 | 0.008 | 0.05 |
| 2416.4 | $9^+ \to 8^+$ | 0.20(7/4) | $9^+_1 \to 8^+_1$ | 0.99 | 1.22 | 0.97 |

[a] Energy of the initial state.

[b] Experimental spin and parity assignments of initial and final states.

[c] Experimental values of $B(\sigma\lambda)$ are given in Weisskopf units. If not labeled with [i] these are $B(M1)$ values. $B(M1)$ and $B(E2)$ values have been derived from the adopted lifetimes and the branching ratios given in Table II. Multipole mixing is neglected. In cases where no parities of the levels could be deduced only $M1$ transitions are considered.

[d] Spin, parity, and number of the states considered in the shell-model calculation of transition probabilities.

[e] Shell-model parameters PARSET-A, configuration space I.

[f] Calculated transition probabilities are given in Weisskopf units. In the calculations of $B(M1)$ and $B(E2)$ values the $g$ factors of the free nucleons and effective charges $1.35e$ for protons and $0.35e$ for neutrons, respectively, have been used.

[g] Shell-model parameters PARSET-B, configuration space I.

[h] Shell-model parameters PARSET-A, configuration space II.

[i] $B(\sigma\lambda)$ values given in this row are $B(E2)$ values.

ground state is too small compared to the experimental value. Furthermore, the sequence of the calculated energies for the $6^-$ and $7^-$ yrast levels is reversed. The calculated levels with spins $12^-$, $13^-$, $14^-$, and $15^-$ have excitation energies and energy separations comparably to the level sequence measured at 5293.4, 5557.2, 6113.4, and 6799.3 keV. This result supports our assignment of negative parity to these states.

Electromagnetic transition probabilities have been calculated using the wave functions obtained with both sets of parameters for the residual interaction (see Table III). For calculating $B(M1)$ values the free-nucleon $g$ factors have been taken. Some $B(E2)$ values have also been calculated using effective charges of $1.35e$ and $0.35e$ [27] for protons and neutrons, respectively. A comparison between experimental and calculated transition probabilities is presented in Table III.

The calculations on the basis of PARSET-A and PARSET-B lead to $B(M1)$ values that are roughly in the same order of magnitude. For transitions between yrast states there are two exceptions, $15_1^+ \rightarrow 14_1^+$ and $10_1^+ \rightarrow 9_1^+$ where in the two parametrizations obviously different states are predicted as yrast states. The large transition probabilities calculated on the basis of both parametrizations for the $M1$ transitions between the states $12_1^-$, $13_1^-$, $14_1^-$, and $15_1^-$ are in qualitative agreement with the experimental data of the $B(M1)$ values between the states on top of the level at 5293.4 keV. For the $M1$ deexcitation of the two yrare states $11_2^+$ and $10_2^+$ as well as for the $B(E2)$ value $10_1^+ \rightarrow 8_1^+$ rather strong discrepancies between the two parametrizations are found. In cases where both calculations lead to similar values of $B(\sigma\lambda)$ these values tend to agree with the experimental data. In most cases where the two predictions deviate strongly from each other the prediction based on PARSET-B is found to be more close to the experimental results than the other prediction. It should be mentioned that the discrepancies concerning the $B(M1)$ values discussed before cannot be removed by the use of effective $g$ factors ($g_s^{\rm eff} = 0.7\, g_s^{\rm free}$ and effective $g$ factors given in [25] for PARSET-A and PARSET-B, respectively) in the calculations.

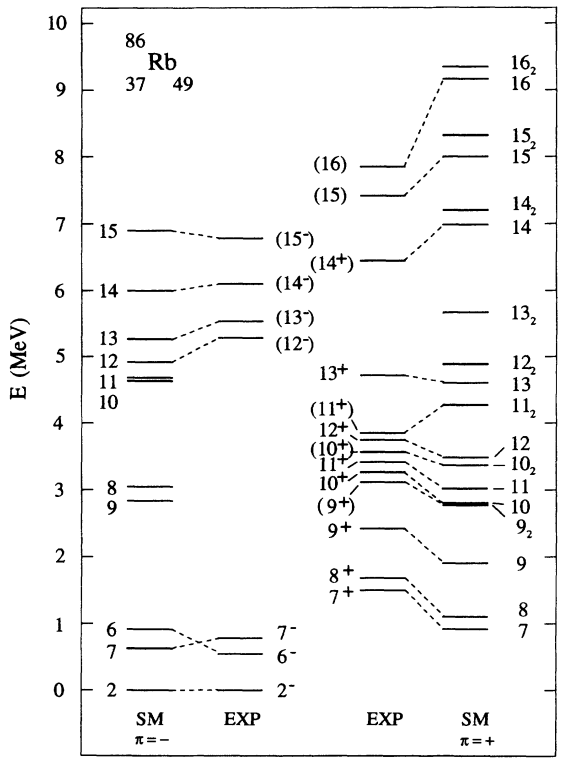


FIG. 8. Comparison of experimental and calculated level energies of $^{86}$Rb using shell-model parameters PARSET-B and configuration space I (see text). From the calculated levels only the ground state, the yrast states with $I^\pi \geq 6^-$ or $I^\pi \geq 7^+$, and the second-lowest states with $I^\pi \geq 9^+$ are shown. Based on the calculated energies only a weak population of the states with $I^\pi = 8^-$ and $9^-$ is expected, and experimental information on these states has not been obtained.

Strong deviations between the transition probabilities obtained in the two shell-model calculations indicate a critical balance between different components of the wave function. The discrepancy between calculated and experimental $B(M1)$ values for the transition between the (16) level at 7859.9 keV and the (15) level at 7412.9 keV might be a hint to considerable admixtures of the $\nu 1d_{5/2}$ shell in the wave functions of these states which is considered in the next subsection.

### B. Results obtained in configuration space II

Compared to configuration space I used in the preceding subsections configuration space II contains a much larger subspace for neutron excitations but a smaller subspace for proton excitations (see Sec. IV B). Consequences of these alterations on the calculated level energies are illustrated in Fig. 9. The influence of the truncation of the proton space can be seen by comparing the level energies given in columns 1 and 2 of Fig. 9 that are obtained by coupling the smaller neutron space (only $0g_{9/2}^9$) to the large and to the reduced proton space, respectively. The limitations in the occupation numbers of the negative-parity proton orbitals result in a wrong prediction of the $2^-$ ground state and of the $6^-$ isomeric state with respect to the positive-parity states. Therefore, the calculated level sequences (columns 1, 2, and 3 in Fig. 9) have been matched to each other at the $7^+$ level. With this normalization a systematic shift of almost all levels to somewhat lower energies is observed in the reduced proton configuration space .

The influence of the increased configuration space for the neutrons can only be demonstrated for the reduced proton space (see columns 2 and 3). The extension of the neutron space leads to rather small alterations of the energies of levels with $I^\pi \leq 14^+$. Comparing the data in columns 1 and 3 a drastic change of the level separations is only observed between the states with $I^\pi = 16^+$ and $I^\pi = 15^+$ which have in configuration space II prevailing contributions of the three-neutron configuration $(0g_{9/2}^8, 1d_{5/2}^1)$. The level energy predicted for the $I$=16$^+$ yrast state in this configuration space is in better accor-

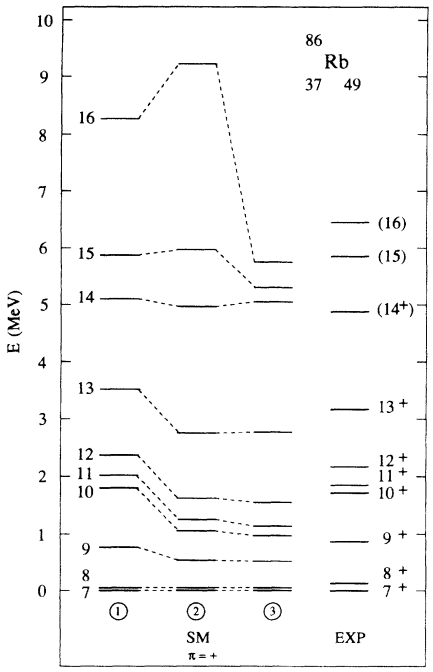


FIG. 9. Comparison of experimental (right column) and calculated level energies of $^{86}$Rb obtained within configuration space I (column 1), within configuration space II excluding excitation of the $\nu 1d_{5/2}$ orbital (column 2) and within configuration space II (column 3) using shell-model parameters PARSET-A (see text).

dance with the experimental data than that obtained in configuration space I (column 1).

The change of the structure of the wave functions between the $14_1^+$ and $15_1^+$ levels is also reflected in the transition probabilities calculated with the wave functions obtained in configuration space II and using PARSET-A (see last right column in Table III). The rather large $B(M1)$ value of about 0.5 W.u. is predicted between the states characterized by three-neutron excitations ($16_1^+$ and $15_1^+$) while the $B(M1)$ value of 0.05 W.u. between the $15_1^+$ and $14_1^+$ levels points to a change of the configuration between these states, which is in qualitative agreement with the experimental data. The $B(M1)$ value of 0.1 W.u. found in this calculation for the yrast transition $14_1^+ \rightarrow 13_1^+$ is in accordance with the experimental result while in both calculations in the configuration space I small $B(M1)$ values are predicted.

The transition probabilities between states with $I^\pi \leq 13^+$ calculated with PARSET-A in the configuration spaces I and II are in most cases of similar magnitudes. Obviously, both configuration spaces overlap rather good for positive-parity states of medium spin.

## VI. SUMMARY

The results of an in-beam study of high-spin states in $^{86}$Rb populated via the reaction $^{82}$Se($^7$Li, $3n$)$^{86}$Rb are presented. A new level scheme of $^{86}$Rb containing states up to 7.9 MeV in excitation energy and spins up to $I=$ (16) has been deduced. Furthermore, for 15 of the levels lifetimes in the ps region have been determined by analyzing the Doppler shift of $\gamma$ rays. Several fast $M1$ transitions with $B(M1) \gtrapprox 0.3$ W.u. have been identified. Shell-model calculations have been carried out to interpret these experimental results. Two different parametrizations of the Hamiltonian have been taken to describe level energies and reduced electromagnetic transition probabilities in $^{86}$Rb. The level energies predicted by both parametrizations are found to be in fair agreement with each other and with the experimental data. Also, most of the experimentally determined electromagnetic transition probabilities could be reasonably well reproduced by the shell-model calculations. However, for some of the $B(M1)$ values considerable deviations between the results obtained in the two calculations have been obtained. The inclusion of neutron particle-hole excitations over the $N$=50 shell gap leads in $^{86}$Rb to an improved description only for the positive-parity states with $I \geq 15$.

## ACKNOWLEDGMENTS

This work was supported by the Deutsche Forschungsgemeinschaft (DFG) and by the Bundesministerium für Forschung und Technologie under Contracts No. Wi 1230/1-1 and No. 06DR103, respectively.

[1] J. Döring , G. Winter, L. Funke, B. Cederwall, F. Lindén, A. Johnson, A. Atac, J. Nyberg, G. Sletten, and M. Sugawara, Phys. Rev. C **46**, R2127 (1992).
[2] I. Hamamoto, Phys. Lett. B **235**, 221 (1990).
[3] J. Döring, L. Funke, W. Wagner, and G. Winter, Z. Phys. A **339**, 425 (1991).
[4] J. Döring, G. Winter, L. Funke, L. Käubler, and W. Wagner, Z. Phys. A **338**, 457 (1991).
[5] H.W. Müller and J. W. Tepel, Nucl. Data Sheets **54**, 527 (1988).
[6] G. Winter and J. Döring, in *Abstracts of the Conference on Nuclear Structure in the Nineties*, edited by N.R. Johnson (Oak Ridge National Laboratory, Oak Ridge, Tennessee, 1990), p. 103.
[7] G. Winter, J. Döring, L. Funke, L. Käubler, R. Schwengner, and H. Prade, Z. Phys. A **332**, 33 (1989).
[8] G. Winter, J. Döring, F. Dönau, and L. Funke, Z. Phys. A **334**, 415 (1989).
[9] G. Winter and J. Döring, Nucl. Instrum. Methods **224**, 327 (1984).
[10] R. Wirowski, Dissertation, Universität zu Köln, 1993.
[11] M. Schimmer, S. Albers, A. Dewald, A. Gelberg, R. Wirowski, and P. von Brentano, Nucl. Phys. **A539**, 527 (1992).

[12] U. Neuneyer, Program KORREL, Universität zu Köln, 1992, unpublished.
[13] J. Lindhard, V. Nielsen, and M. Scharff, Mat. Fys. Medd. Dan. Vid. Selsk. **36**, 10 (1968).
[14] L. Lühmann, M. Debray, K.P. Lieb, W. Nazarewicz, B. Wörmann, J. Eberth, and T. Heck, Phys. Rev. C **31**, 825 (1985).
[15] P.M. Endt, At. Data Nucl. Data Tables **23**, 547 (1979).
[16] D. Zwarts, Comput. Phys. Commun. **38**, 365 (1985).
[17] G. Winter, R. Schwengner, J. Reif, H. Prade, L. Funke, R. Wirowski, N. Nicolay, A. Dewald, P. von Brentano, H. Grawe, and R. Schubart, Phys. Rev. C **48**, 1010 (1993).
[18] X. Ji and B.H. Wildenthal, Phys. Rev. C **37**, 1256 (1988).
[19] R. Gross and A. Frenkel, Nucl. Phys. **A267**, 85 (1976).
[20] P.C. Li, W.W. Daehnick, S.K. Saha, J.D. Brown, and R.T. Kouzes, Nucl. Phys. **A469**, 393 (1987).
[21] P.C. Li and W.W. Daehnick, Nucl. Phys. **A462**, 26 (1987).
[22] K. Muto, T. Shimano, and H. Horie, Phys. Lett. **135B**, 349 (1984).
[23] P.W.M. Glaudemans, P.J. Brussaard, and B.H. Wildenthal, Nucl. Phys. **A102**, 593 (1967).
[24] J. Blomqvist and L. Rydström, Phys. Scr. **31**, 31 (1985).
[25] J. Sinatkas, L.D. Skouras, D. Strottman, and J.D. Vergados, J. Phys. G **18**, 1377 (1992); **18**, 1401 (1992).
[26] T.T.S. Kuo and G.E. Brown, Nucl. Phys. **85**, 40 (1966); Nucl. Phys. **A114**, 241 (1968).
[27] M.K. Kabadiyski, F. Cristancho, C.J. Gross, A. Jungclaus, K.P. Lieb, D. Rudolph, H.Grawe, J. Heese, K.-H. Maier, J. Eberth, S. Skoda, W.-T. Chou, and E.K. Warburton, Z. Phys. A **343**, 165 (1992).